Article

Not peer-reviewed version

Inhibitory Effects of Human β-Defensin 3 on *Porphyromonas gingivalis* Lipopolysaccharide-Induced Il-1β Production by Bv-2 Microglia through Suppression of Cathepsins B and L

Erika Innoue , Shiyo Minatozaki , Sachi Shimizu , Sayaka Miyamoto , Misato Jo , Junjun Ni , Hidetoshi Tozaki-Saitoh , Kosuke Oda , Saori Nonaka , Hiroshi Nakanishi *

Posted Date: 26 December 2023

doi: 10.20944/preprints202312.1924.v1

Keywords: BV-2 microglia; cathepsin B; CA-074Me; human β-defensin 3; interleukin-1β; lipopolysaccharide; nuclear factor-κB; outer membrane vesicles; Prophyromonas gingivalis

Article

Inhibitory Effects of Human β-Defensin 3 on *Porphyromonas gingivalis* Lipopolysaccharide-Induced IL-1β Production by BV-2 Microglia Through Suppression of Cathepsins B and L

Erika Inoue [1,†], Shiyo Minatozaki [1,†], Sachi Shimizu [1], Sayaka Miyamoto [1], Misato Jo [1], Junjun Ni [2], Hidetoshi Tozaki-Saitoh [3], Kosuke Oda [4], Saori Nonaka [4] and Hiroshi Nakanishi [4,*]

[1] Yasuda Women's University, Hiroshima 731-0153, Japan; 19141105@st.yasuda--u.ac.jp (E.I); 19141237@st.yasuda-u.ac.jp (S.M.); 20141218@st.yasuda-u.ac.jp (S.S.); 20141243@st.yasuda-u.ac.jp (S.M.); 20141219@st.yasuda-u.ac.jp (M.J.)

[2] Key Laboratory of Molecular Medicine and Biotherapy, School of Life Science, Beijing Institute of Technology, Beijing 100081, China; nijunjun@bit.edu.cn (J.N.)

[3] Department of Pharmaceutical Sciences, School of Pharmacy at Fukuoka, International University of Health and Welfare, Okawa, Fukuoka 831-8501, Japan; saitoh@iuhw.ac.jp (H.T-S)

[4] Department of Pharmacology, Faculty of Pharmacy, Yasuda Women's University, Yasuhigashi, Hiroshima 731-0153, Japan; oda-k@yasuda-u.ac.jp (K.O.); nonaka-s@yasuda-u.ac.jp (S.N.); nakanishi-h@yasuda-u.ac.jp (H.N.)

* Correspondence: nakanishi-h@yasuda-u.ac.jp (H.N.)

† These authors contributed equally to this work.

Abstract: Cathepsin B (CatB) is thought to be essential for the induction of *Porphyromonas gingivalis* lipopolysaccharide (*Pg* LPS)-induced Alzheimer's disease- like pathologies in mice, including interleukin-1β (IL-1β) production and cognitive decline. However, little is known about the role of CatB in *Pg* virulence factor-induced IL-1β production by microglia. We first subjected IL-1β-luciferase reporter BV-2 microglia to inhibitors of Toll-like receptors (TLRs), IκB kinase, and the NLRP3 inflammasome following stimulation with *Pg* LPS and outer membrane vesicles (OMVs). To clarify the involvement of CatB, we used several known CatB inhibitors, including CA-074Me, ZRLR, and human β-defensin 3 (hBD3). IL-1β production in BV-2 microglia induced by *Pg* LPS and OMVs was significantly inhibited by the TLR2 inhibitor C29 and the IκB kinase inhibitor wedelolactonne, but not by the NLRPs inhibitor MCC950. Both hBD3 and CA-074Me significantly inhibited *Pg* LPS-induced IL-1β production in BV-2 microglia. Although CA-074Me also suppressed OMV-induced IL-1β production, hBD3 did not inhibit it. Furthermore, both hBD3 and CA-074Me significantly blocked *Pg* LPS-induced nuclear NF-κB p65 translocation and IκBα degradation. In contrast, hBD3 and CA-074Me did not block OMV-induced nuclear NF-κB p65 translocation or IκBα degradation. Furthermore, neither ZRLR, a specific CatB inhibitor, nor shRNA-mediated knockdown of CatB expression had any effect on *Pg* virulence factor-induced IL-1β production. Interestingly, phagocytosis of OMVs by BV-2 microglia induced IL-1β production. Finally, the structural models generated by AlphaFold indicated that hBD3 can bind to the substrate-binding pocket of CatB, and possibly CatL as well. These results suggest that *Pg* LPS induces CatB/CatL-dependent synthesis and processing of pro-IL-1β without activation of the NLRP3 inflammasome. In contrast, OMVs promote the synthesis and processing of pro-IL-1β through CatB/CatL-independent phagocytic mechanisms. Thus, hBD3 can improve the IL-1β-associated vicious inflammatory cycle induced by microglia through inhibition of CatB/CatL.

Keywords: BV-2 microglia; cathepsin B; CA-074Me; human β-defensin 3; interleukin-1β; lipopolysaccharide; nuclear factor-κB; outer membrane vesicles; *Prophyromonas gingivalis*

 doi:10.20944/preprints202312.1924.v1

1. Introduction

Microglia-mediated neuroinflammation is an important component of Alzheimer's disease (AD) pathogenesis and has been implicated in neurodegeneration [1–3]. Interleukin-1β (IL-1β) is a potent proinflammatory cytokine involved in many important cellular functions. The release of IL-1β is a critical step in inflammation through the induction of other proinflammatory cytokines and chemokines [4,5]. IL-1β is chronically upregulated in AD and believed to play a role in the vicious inflammatory cycle that drives AD pathology [6]. A two-step process is generally necessary for IL-1β production. First step is the synthesis of pro-IL-1β, and second step is the processing of synthesized pro-IL-1β. The TLR-dependent signals first activate nuclear factor-κB (NF-κB) to lead pro-IL-1β synthesis. The Nod-like receptor (NLR) family pyrin domain containing 3 (NLRP3) inflammasome then undergoes post-translational modifications that license its activation. The activation signals activate the NLRP3 inflammasome with subsequent activation of pro-caspase-1, which in turn catalyzes the cleavage of pro-IL-1β.

Activation signals are provided by a variety of stimuli and multiple molecular or cellular events, including K^+ efflux, mitochondrial dysfunction with reactive oxygen species (ROS) generation, and lysosomal damage with cathepsin B (CatB; EC 3.4.22.1) leakage. Several studies have suggested a CatB/NLRP3/caspase-1-dependent pathway for pro-IL-1β processing in BV-2 microglia [7] and THP-1 cells [8], and the roles of multiple cathepsins in NLRP3 activation have also been implicated in macrophages/microglia [9,10]. However, we previously reported a potential NLRP3-independent role of autolysosomal CatB in pro-caspase-1 activation and subsequent IL-1β secretion by microglia following stimulation with chromogranin A [11,12]. Therefore, there are at least three different pathways for pro-IL-1β processing, with a special focus on the role of CatB, depending on the stimulating reagents and cell types: (1) a CatB/NLRP3/ caspase-1-dependent pathway, (2) a CatB/caspase-1-dependent, but NLRP3-independent pathway, and (3) a CatB and other cysteine cathepsins/NLRP3/ caspase-1-dependent pathway. In addition to pro-IL-1β processing, there is some evidence demonstrating that CatB is also involved in pro-IL-1β synthesis through the degradation of IκBα, an endogenous inhibitor of NF-κB in macrophages/microglia at the late stage of inflammation [9,13–17].

The emerging role of microbes and innate immune pathways in AD pathology suggests that antimicrobial peptides may be effective as early therapeutic intervention in future clinical trials [18,19]. The salivary proteome contains a complex mixture of over 45 antimicrobial proteins and peptides, including human defensins, histatins and cathelicidin hCAP18/LL-37 [20]. Human β-defensins (hBDs) are small, cationic antimicrobial peptides produced by the oral mucosa and salivary glands. We previously reported that hBD3 strongly suppresses the delayed type of inflammatory responses by microglia following treatment with lipopolysaccharide (LPS) derived from *Porphyromonas gingivalis* (*Pg*), a major pathogen of chronic periodontitis. hBD3 suppresses *Pg* LPS-induced NF-κB activation through inhibition of CatB and cathepsin L (CatL; EC 3.4.22.15) [21]. Furthermore, we first reported that chronic systemic exposure to *Pg* LPS induces AD-like pathologies, including microglia-mediated neuroinflammation and cognitive decline in middle-aged mice, but not in CatB-deficient mice [22].

However, whether or not hBD3 and CatB inhibitors can suppress *Pg* virulence factor-induced IL-1β production by microglia remains unclear. In addition to *Pg* LPS, chronic oral gavage with outer membrane vesicles (OMVs) secreted from *Pg* also induced AD-like pathologies in middle-aged mice [23]. In the present study, we have thus attempted to clarify effects of hBD3 and CatB inhibitors on the IL-1β production by microglia following stimulation with *Pg* LPS and OMVs.

2. Materials and Methods

2.1. Reagents

hBD3, CA-074Me, KYT-1 and KYT-36 were purchased from the Peptide Institute Inc (Osaka, Japan), and Z-Arg-Leu-Arg-α-aza-glycil-Ile-Val-OMe (ZRLR) was synthesized by Peptide Institute Inc. Standard *Pg* LPS was purchased from InvivoGen (San Diego, CA, USA). TAK-242 and C29 were

 doi:10.20944/preprints202312.1924.v1

purchased from MedChem Express (Monmouth Junction, NJ, USA). MCC950 was purchased from Adipogen Life Sciences, Inc (San Diego, CA, USA). Wedelolactone was purchased from Tokyo Chemical Industry Co., Ltd (Tokyo, Japan).

2.2. Cell culture

The BV-2 cells, a murine microglial cell line [24], and a well-accepted alternative to primary microglia [25,26], were used in this study. BV-2 microglia were cultured in Dulbecco's modified Eagle's medium (Thermo Fisher Scientific, Waltham, MA, USA) supplemented with 5% fetal bovine serum (FBS), penicillin, and streptomycin. To establish NanoLuc (Nluc) probe-expressing cells (Nluc reporter BV-2 microglia), we infected the cells with a lentiviral vector carrying the Nluc probe, as described previously [27], during routine culturing. After two passages, the cells were detached using Accutase (Nacalai Tesque, Kyoto, Japan), and EGFP-positive cells were sorted using a BD FACSAria III cell sorter (BD Life Sciences, San Jose, CA, USA). In this assay system, the Nluc luciferase gene was designed to be induced by the promoter activity of the *Il1b* gene, and luciferase activity was only induced when proteolytic processing of pro-IL-1β occurred because the Nluc luciferase was fused with the sequence of IL-1β (*Il1b* 17-216), which has been subjected to proteolytic processing of various proteases including inflammasome-mediated caspase-1 [28]. Furthermore, the *C*-terminus of *Il1b* 17-216 was fused with two protein destabilization sequences (hCL1 and hPEST), allowing for rapid proteasome-mediated degradation. Thus, the Nluc luciferase protein is retained only when the proteolytic processing of IL-1β is successful, as it can be escape proteasome degradation.

2.3. The measurement of the luciferase activity (RLU)

Nluc reporter BV-2 microglia were plated in 96-well culture plates at a density of 3×10^4 cells per well. After overnight culture, drug treatments were performed, and luciferase activity following treatment with *Pg* LPS (10 μg/mL) or OMVs (150 μg/mL) for 1 h was measured using a luminometer (GloMax; Promega Corp., Madison, WS, USA) with a Nano-Glo® luciferase assay system (N1110; Promega Corp.) according to the manufacturer's protocol. The luciferase activity (RLU) in BV-2 microglia induced by *Pg* LPS or OMVs was then measured. Each treatment was repeated in triplicate on the same plate, and at least three independent experiments were performed.

2.4. Bacterial culture and isolation of OMVs

Pg ATCC33277 (wild-type; WT), Kgp-deficient mutant strain (KDP129), and a Kgp- and Rgp (both RgpA and RgpB)-deficient mutant strain (KDP136) were maintained on blood agar plates containing 40 mg/mL trypto-soya agar (Nissui Pharmaceutical, Tokyo, Japan), 5 mg/mL brain heart infusion (BHI) medium (Becton, Dickinson and Company, Franklin Lakes, NJ, USA), 1 mg/mL cysteine (Wako Pure Chemical Industries, Osaka, Japan), 5 μg/mL hemin (Sigma-Aldrich, St. Louis, MO, USA), 0.5 μg/mL menadione (Sigma-Aldrich), and 5% defibrinated sheep blood (Nippon Bio-Test Laboratories, Tokyo, Japan) in a Bactron anaerobic chamber (Shel Lab, Cornelius, OR, USA) at 5% CO_2, 5% H_2, and 90% N_2.

For immunostaining experiments, OMVs were isolated as described previously [29]. In brief, the bacteria were grown in enriched BHI broth containing 37 mg/mL BHI medium, 2.5 mg/mL yeast extract, 1 mg/mL cysteine, 5 μg/mL hemin, and 0.5 μg/mL menadione. The culture medium was centrifuged at 2800×*g* for 15 min at 4 °C to remove bacterial cells. The supernatant was filtered through a Millipore filter (pore size, 0.22 μm). The filtered supernatant (8 mL) was concentrated to 1 mL using an ultrafiltration column at 10 K (Apro Science, Tokushima, Japan). The concentrate was mixed with the Total Exosome Isolation Reagent (Thermo Fisher Scientific Inc.) and incubated overnight at 4 °C. The samples were then centrifuged at 10,000×*g* for 60 min at 4 °C. The OMVs fraction was dissolved in 100 μL of phosphate-buffered saline (PBS) and used for the experiments.

In other experiments, OMVs were prepared by ultracentrifugation as described previously [30]. In brief, *Pg* was grown in enriched BHI broth and then removed from the culture by centrifugation at 10,000×*g* for 30 min at 4 °C. The supernatant was filtered through a Millipore filter (pore size, 0.22

 doi:10.20944/preprints202312.1924.v1

μm). OMVs were collected as pellets by ultracentrifugation of the culture supernatant at 100,000×*g* for 3 h at 4 °C and then dissolved in PBS.

2.5. Fluorescence imaging of cellular localization of OMVs

OMVs from the WT and KDP136 strains (75 μg of total protein) prepared with the Total Exosome Isolation Reagent were incubated with 5 μM Cy5 Mono NHS Ester (Lumiprobe Corporation, Cockeysville, MD, USA) for 90 min at 37 °C. The labelled OMVs were collected by centrifugation (10,000×g for 30 min at 4 °C), dissolved in PBS, and then centrifuged at 10,000×g for 30 min at 4 °C to remove the unincorporated dye. The precipitated labelled OMVs were dissolved in FBS-free DMEM (0.5 mL). To observe the cellular localization of Cy5-labelled OMVs, Nluc reporter BV-2 microglia (2×10^4 cells/well) were cultured on collagen-coated cover glass in 24-well plates at 37 °C for 1 day and then incubated with FBS-free DMEM containing Cy5-labelled OMVs (150 μg of protein/mL) for 1 h. After incubation, the cells were fixed with 4% (w/v) paraformaldehyde for 15 min and then permeabilized with PBS containing 0.2% (v/v) Triton X-100. After washing with PBS, the cells were incubated with Acti-stain 488 phalloidin (a F-actin detecting dye, Cytoskeleton, Inc., Denver, CO, USA) and Hoechst 33342 (ThermoFisher Scientific) to visualize the cells. Fluorescence images were obtained using a confocal laser-scanning microscope (CLSM; FV1000, Olympus, Tokyo, Japan).

2.6. Trasfection of CatB shRNA

Nluc reporter BV-2 microglia were transfected to CatB shRNA or control shRNA lentiviral particle (Santa Cruz Biotechnology, Inc., Dallas, TX, USA) according to the manufacture's transfection protocol. In brief, Nluc reporter BV-2 microglia were cultured with complete optimal medium in a 12-well plate (3×10^5 cells/well) 24 h prior to lentiviral infection. Media were removed from the plate wells and replaced with 1 mL of polyberene/media mixture (5 μg/mL) per well. CatB or control shRNA lentiviral particles were then added and incubated overnight. The cells were cultured for an additional 48 h in complete medium without polybrene. Stable clones expressing CatB shRNA (Nluc reporter CatB-knockdown BV-2 microglia) or control shRNA were selected using puromycin dihydrochloride (6 μg/mL).

2.7. Fluorescence imaging of enzymatic activities of CatB and CatL

BV-2 microglia were stained with the cell-permeable fluorescently labeled CatB substrate z-Arg-Arg-cresyl violet or CatL substrate z-Phe-Arg-cresyl violet according to the manufacturer's instructions (cv-CatB detection kit and cv-CatL detection kit; Enzo Life Sciences, Inc., Farmingdale, NY, USA). Chamber slides containing stained live cells were then mounted in PBS. Fluorescence images were obtained using CLSM (FV1000, Olympus).

2.8. Nuclear NF-κB p65 translocation

BV-2 microglia were treated with *Pg* LPS (10 μg/mL) or OMVs (150 μg/mL) for 1 h in the absence or presence of hBD3 (1 μM) or CA-074Me (30 μM), and were fixed with 4% paraformaldehyde. hBD3 and CA-074Me were pre-incubated with BV-2 microglia for 2 and 4 h, respectively. They were then incubated with a rabbit anti-NF-κB p65 IgG antibody (Abcam, Cambridge, UK). After washing with PBS, the cells were incubated with donkey anti-rabbit Alexa 555 (ThermoFisher Scientific), Hoechst 33342, and mounted in Vectashield anti-fading medium (Vector Laboratories, Newark, CA, USA). Fluorescence images were captured using CLSM (FV1000, Olympus). The line plot profile was analyzed using the Image J software program.

2.9. Immunoblotting analyses

For detecting IκB*α* and β-actin, BV-2 microglia were used. WT and CatB-KD BV-2 microglia were used to detect CatB and GAPDH. Cells were seeded in a 6 cm petri dish at a density of 2.5-3.3×10^6 cells/dish for 1 day. After treatment with *Pg* LPS or OMVs in the absence or presence of hBD3 (1 μM) or CA-074Me (30 μM), the cells were lysed with RIPA buffer, consisting of 10 mM Tris-HCl

 doi:10.20944/preprints202312.1924.v1

(pH 7.5), 1% (*v*/*v*) NP-40, 0.1% (*w*/*v*) sodium deoxycholate, 0.1% (*w*/*v*) sodium dodecyl sulfate (SDS), 150 mM NaCl, 1 mM EDTA, and protease inhibitor cocktail (Nacalai Tesque, Kyoto, Japan), and then cell lysates were subjected to 10% (*w*/*v*) SDS-polyacrylamide gel electrophoresis. The proteins on the SDS–polyacrylamide gels were then transferred to nitrocellulose membranes. After blocking with Blocking One (Nacalai Tesque), the membranes were incubated with rabbit anti-IκBα (Abcam), rabbit anti-β-actin (GENETEX, Irvine, CA), rabbit anti-CatB antibodies (Abcam), and rabbit anti-GAPDH (Proteintech, Tokyo, Japan) antibodies at 4°C overnight. After washing, the membranes were incubated with horseradish peroxidase (HRP)-labeled anti-rabbit IgG antibodies (GE Healthcare, Tokyo, Japan) for 1 h at room temperature. Membrane-bound HRP-labeled antibodies were detected using the Amasham ECL Western blotting detection reagent and analysis system (GE Healthcare) with an imaging analyzer (LAS-4000, Fujifilm, Tokyo, Japan). Signal intensities were determined using the Image Lab 6.0.1 software program (Bio-Rad, Hercules, CA, USA).

2.10. AlphaFold predictions

The AlphaFold models were predicted using the AlphaFold v2.0 algorithm on the Colab server (https://colab.research.google.com/github/ sokrypton/ColabFold/blob/ main/AlphaFold2.ipynb), accessed on November 20, 2023 [31]. Predictions were performed with default multiple sequence alignment generation using the MMSeqs2 server, with 48 recycles, and templates (homologous structures). The best of the five predicted models (rank 1) computed by AlphaFold was considered in the present work.

2.11. Statistical analyses

Data are presented as the mean ± standard error (SE). Statistical analyses of the results were performed using a one-way analysis of variance (ANOVA) with a post-hoc Tukey's test and Student's *t*-test using the GraphPad Prism8 (GraphPad Software, Inc., CA, USA) software package. $P<0.05$ was considered to indicate statistical significance.

3. Results

3.1. Effects of inhibitors for TLR4, TLR2, IκB kinase and NLRP3 inflammasome on the IL-1β production by BV-2 microglia following stimulation with Pg LPS and OMVs.

To assess the involvement of TLRs in the IL-1β production by BV-2 microglia following stimulation with *Pg* LPS and OMVs, effects of TAK-242 and C29, specific inhibitors of TLR4 and TLR2, respectively, on IL-1β production were examined by measuring the luciferase activities of the Nluc reporter BV-2 microglia. *Pg* LPS-induced luciferase activity was almost completely suppressed by C29 (100 μM), but not by TAK-242 (1 μM) (Figure 1A). OMV-induced luciferase activity was significantly but not completely suppressed by C29 (100 μM) (Figure 1B). TAK-242 (1 μM) had no significant effect. Furthermore, wedelolactone (30 μM), an IκB kinase inhibitor, significantly and completely inhibited the mean luciferase activity induced by *Pg* LPS and OMVs (Figure 1C). In contrast, MCC950 (10 μM), an NLRP3 inflammasome inhibitor, had no effect on the mean luciferase activity induced by *Pg* LPS or OMVs (Figure 1D).

Preprints (www.preprints.org) | NOT PEER-REVIEWED | Posted: 26 December 2023 doi:10.20944/preprints202312.1924.v1

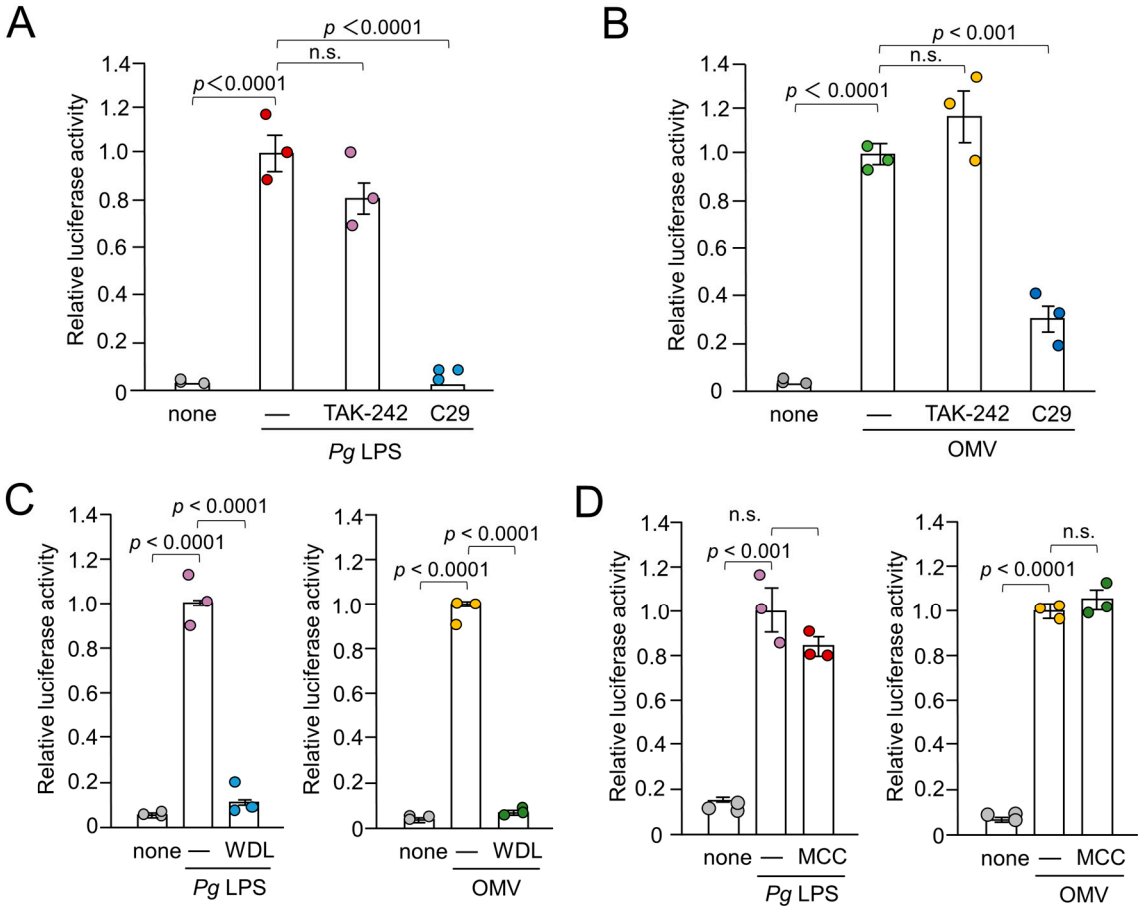

Figure 1. Effects of inhibitors for TLR4, TLR2, IκB kinase and NRP3 inflammasome on the luciferase activity of the IL-1β probe in BV-2 microglia following stimulation with *Pg* LPS and OMVs for 1 h. (**A**), (**B**) The mean relative luciferase activity of the IL-1β probe induced by *Pg*LPS (**A**) and OMVs (**B**) in the absence or presence of the TLR4 inhibitor TAK-242 or the TLR2 inhibitor C29. (**C**) The mean relative luciferase activity of the IL-1β probe induced by *Pg* LPS and OMVs in the absence or presence of the IκB kinase inhibitor wedelolactone (WDL). (**D**). The mean relative luciferase activity of the IL-1β probe induced by *Pg* LPS and OMVs in the absence or presence of the NLRP3 inflammasome inhibitor MCC950 (MCC). The data relative to the values in *Pg* LPS or OMV-treated cells are presented as the mean ± SE of three independent experiments, and *p* values were calculated using a one-way ANOVA with a post-hoc Tukey's test. A value of $p < 0.05$ was considered to indicate statistical significance.

3.2. Possible involvement of phagocytosis of OMVs by BV-2 microglia in the IL-1β production

We next examined the possible phagocytosis and cellular localization of Cy5-labeled OMVs by BV-2 microglia. F-actin localized around the cell periphery. Cy5-labeled OMVs were phagocytosed by BV-2 microglia and accumulated as coarse granular aggregates, suggesting endosomal/ lysosomal localization (Figure 2A, C). Vertical optical sections of BV-2 microglia clearly showed the intracellular localization of OMVs.

3.3. Possible involvement of gingipains in IL-1β production by BV-2 microglia following treatment with OMVs

After secretion through the type IX system, gingipains, a group of lysine (Kgp)- and arginine (RgpA)-specific cysteine proteases, attach to anionic LPS located on the outer membrane surface of *Pg* [32]. Therefore, in addition to LPS, gingipains attached to the surface of OMVs may also be associated with the IL-1β production. KYT-1 (10 μM, an Rgp inhibitor), KYT-36 (10 μM, a Kgp

Preprints (www.preprints.org) | NOT PEER-REVIEWED | Posted: 26 December 2023 doi:10.20944/preprints202312.1924.v1

inhibitor), and the combination thereof had no effect on OMV-induced luciferase activity in BV-2 microglia (Figure 2B). Furthermore, OMVs prepared from KDP129, a Kgp-deficient mutant strain, induced luciferase activity in BV-2 microglia to a level similar to that of the WT. In contrast, OMVs prepared from KDP136, a Kgp- and Rgp-deficient mutant strain, did not induce luciferase activity in BV-2 microglia. Furthermore, it was also noted that BV-2 micoglia did not phagocytose Cy5-labeled OMVs prepared from KDP136 (Figure 2C).

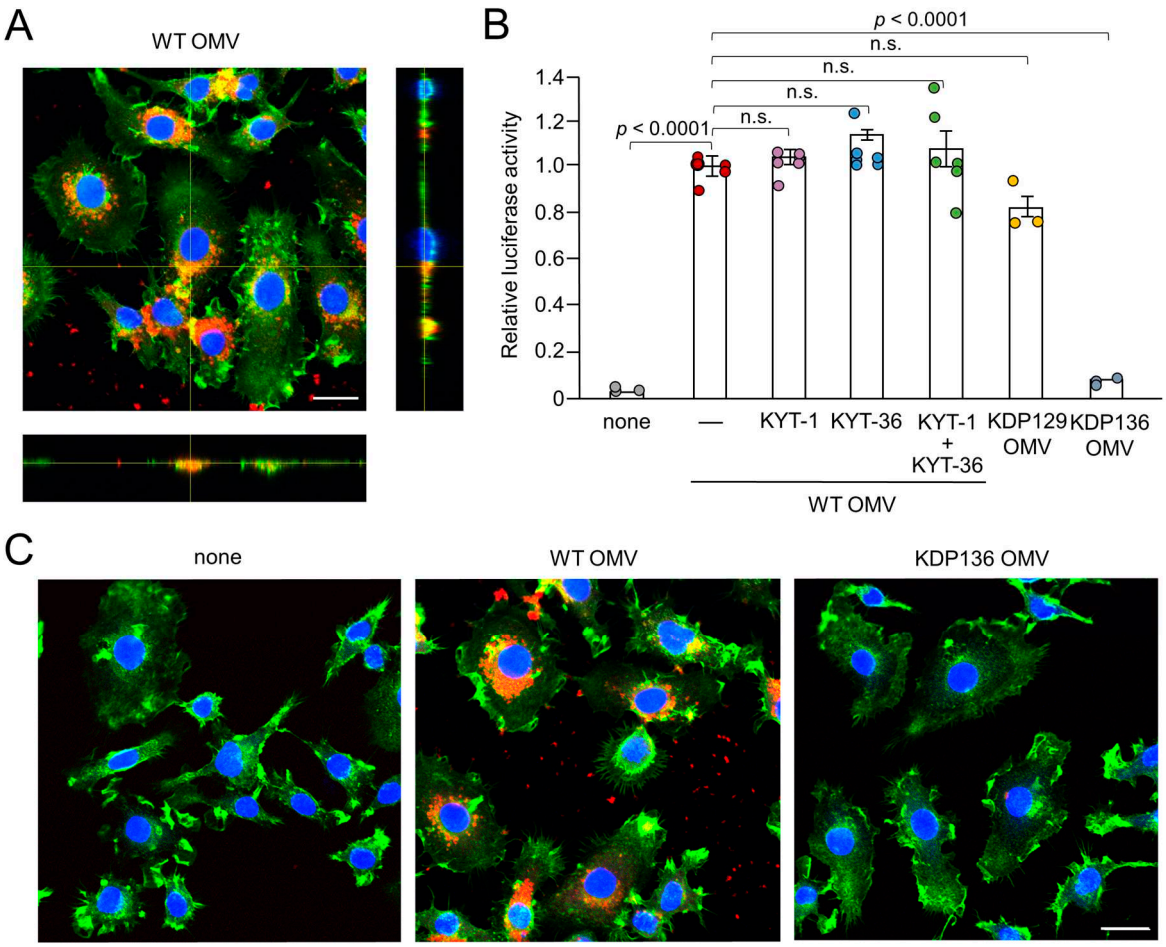

Figure 2. Phagocytosis of OMVs by BV-2 microglia and possible involvement of gingipains in OMV-induced IL-1β production. (**A**) CLSM images of BV-2 microglia after treatment with Cy5-labelled OMVs for 1 h prepared from wild-type strain (WT OMV). F-actin and nuclei were visualized with Acti-stain 488 phalloidin (green) and Hoechst 33342 (blue), respectively. Bottom and right rectangular panels represent z-stack images. Scale bar = 20 μm. (**B**) The mean relative luciferase activity of the IL-1β probe induced by OMVs for 1 h after pharmacological and genetic inhibition of gingipains. KYT-1: Rgp inhibitor; KYT-136: Kgp inhibitor; KDP129: OMVs prepared from Kgp mutant strain; KDP136: OMVs prepared from Rgp and Kgp mutant strain. The data relative to the values in WT OMV-treated cells are presented as the mean ± SE of three-six independent experiments, and *p* values were calculated using a one-way ANOVA with a post-hoc Tukey's test. A value of $p<0.05$ was considered to indicate statistical significance. (C) CLSM images of BV-2 microglia after treatment with Cy5-labelled OMVs (red) prepared from wild-type (WT OMV) and gingipain-null mutant KDP136 strains for 1 h. F-actin and nuclei were visualized with Acti-stain 488 phalloidin (green) and Hoechst 33342 (blue), respectively. Scale bar = 20 μm.

3.4. Effects of pharmacological and genetic inhibition of CatB on IL-1β production by BV-2 microglia following stimulation with Pg LPS and OMVs

Next, we examined the effects of CA-074Me, hBD3 and ZRLR on the IL-1β production by measuring the luciferase activity. Both CA-074Me (10 μM) and hBD3 (1 μM) significantly inhibited

Preprints (www.preprints.org) | NOT PEER-REVIEWED | Posted: 26 December 2023 doi:10.20944/preprints202312.1924.v1

luciferase activity induced by *Pg* LPS in BV-2 microglia (Figure 3A). However, ZRLR (10 μM), a membrane-permeable specific inhibitor of CatB [33], did not inhibit luciferase activity. CA-074Me (10 μM) also significantly inhibited OMV-induced luciferase activity in BV-2 microglia, neither hBD3 (1 μM) nor ZRLR (10 μM) inhibited this activity (Figure 3B).

We examined the possible inhibitory effects of CA-074Me and ZRLR on the enzymatic activities of CatB and CatL in BV-2 microglia using cell-permeable, fluorescently labeled substrates, z-Arg-Arg-cresyl violet and z-Phe-Arg-cresyl violet, respectively. The fluorescent cresyl violet group was designed to be dequenched upon cleavage of dipeptides by CatB or CatL. CA-074Me (10 μM) markedly reduced the enzymatic activity of both CatB and CatL in BV-2 microglia. In contrast, ZRLR (10 μM) markedly reduced the fluorescent signal of CatB, but not that of CatL (Figure 4).

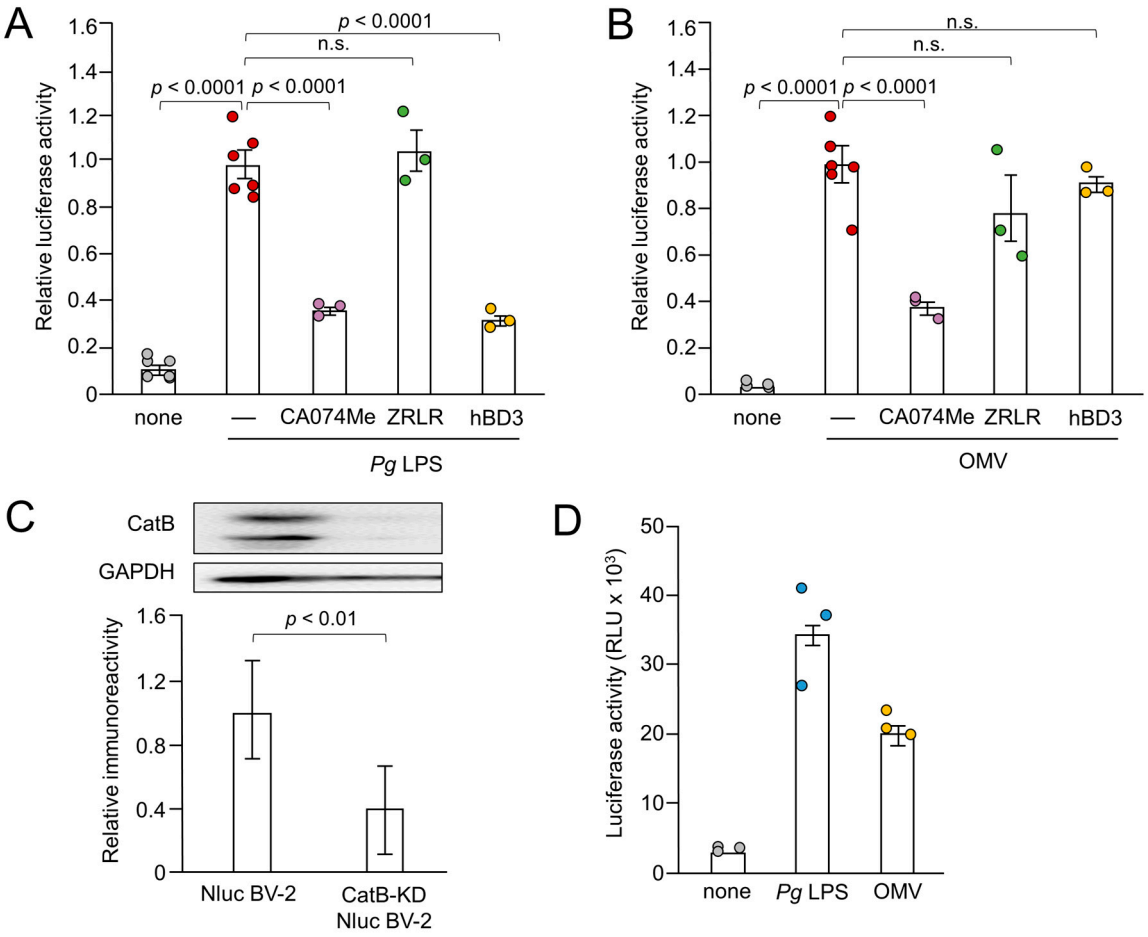

Figure 3. Effects of pharmacological and genetic inhibition of CatB on IL-1β production by BV-2 microglia following stimulation with *Pg* LPS and OMVs. (**A**), (**B**) The mean relative luciferase activity of the IL-1β probe induced in BV-2 microglia following treatment with *Pg* LPS (**A**) and OMVs (**B**) after treatment with hBD3 (1 μM), CA-074Me (10 μM) or ZRLR (10 μM). The data are presented as the mean ± SE of 3-6 independent experiments, and *p* values were calculated using a one-way ANOVA with a post-hoc Tukey's test. A value of $p < 0.05$ was considered to indicate statistical significance. (**C**) The mean values of CatB intensity, which were detected by the immunoblot shown, were measured in Nluc reporter BV-2 microglia (Nluc BV-2) and Nluc reporter CatB-knockdown BV-2 microglia (CatB-KD Nluc BV-2) and normalized against the signal of GAPDH. The data are presented as the mean ± SE of three independent experiments, and the *p* value was calculated using Student's *t*-test. (**D**) The mean luciferase activity (RLU) of the IL-1β probe induced by *Pg* LPS or OMV in CatB-KD Nuc BV-2 microglia. The data are presented as the mean ± SE of 3 independent experiments.

Preprints (www.preprints.org) | NOT PEER-REVIEWED | Posted: 26 December 2023 doi:10.20944/preprints202312.1924.v1

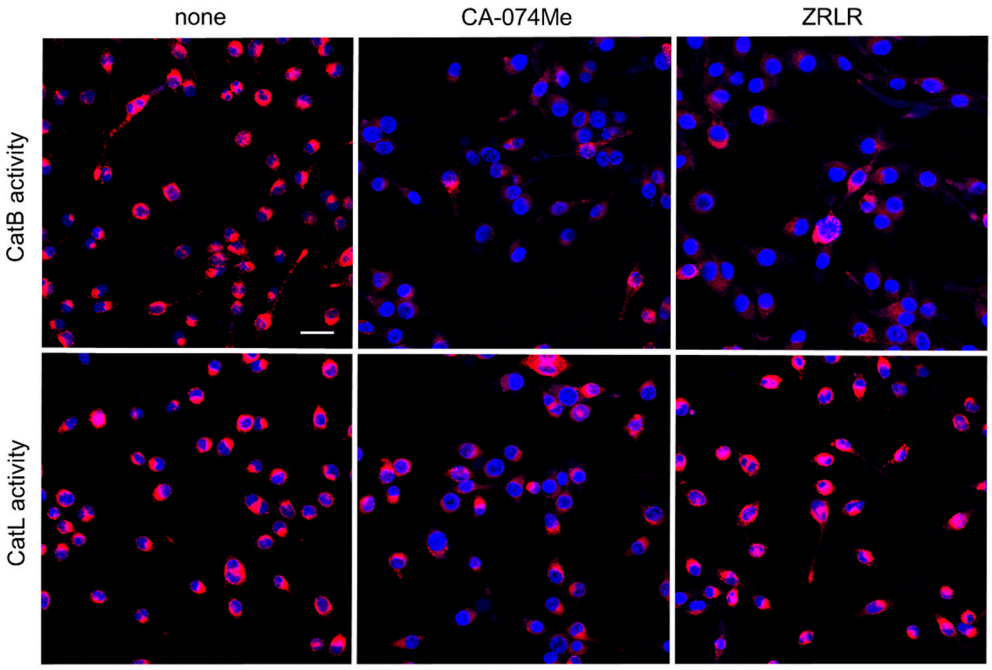

Figure 4. Enzymatic activities of CatB and CatL visualized using the cell-permeable, fluorescently labeled substrates, z-Arg-Arg-cresyl violet and z-Phe-Arg-cresyl violet, respectively, in the absence (none) and presence of CA-074Me (10 μM) or ZRLR (10 μM). Scale bar = 40 μm.

We further examined the effect of the genetic inhibition of CatB on the IL-1β production by BV-2 microglia following stimulation with *Pg* LPS and OMVs. As shown in Figure 3C, mature CatB was detected in a single-chain form and in the heavy chain of the two-chain form. The mean intensity of CatB immunoreactivity was significantly lower in BV-2 microglia after stable infection with CatB shRNA lentiviral particles than non-infected Nluc reporter BV-2 microglia (Figure 3C). The mean luciferase activity (RLU) of the IL-1β probe in BV-2 microglia following stimulation with *Pg* LPS and OMVs was 33×10^3 (n=3) and 21×10^3 (n=3), respectively (Figure 3D). The mean RLU measured in Nluc reporter BV-2 microglia (WT) following treatment with *Pg* LPS and OMVs was 15×10^3 (range: 7-22×10^3, n=15) and 18×10^3 (range: 8-26×10^3, n=21), respectively. Therefore, CatB knockdown did not affect IL-1β production by BV-2 microglia following stimulation with *Pg* LPS or OMVs.

3.5. Effects of CA-074Meand hBD3 on Pg LPS-induced nuclear NF-κB p65 translocation in BV-2 microglia following stimulation with Pg LPS and OMVs

The promoter regions of both IL-1β genes have a putative NF-κB binding site. Therefore, abrogation of NF-κB activation is plausible mechanisms underlying the inhibitory the effects of CA-074Me and hBD3 on pro-Il-1β synthesis. Thus, we examined effects of CA-074Me and hBD3 on nuclear NF-κB p65 translocation following treatment with *Pg* LPS and OMVs. Both hBD3 (1 μM) and CA-074Me (10 μM) inhibited *Pg* LPS-induced nuclear NF-κB p65 translocation in BV-2 microglia (Figure 5A,B). In contrast, neither hBD3 (1 μM) nor CA-074Me (30 μM) inhibited OMV-induced nuclear NF-κB p65 translocation (Figure 5A,B).

3.6. Effects of hBD3 and CA-074Me on the degradation of IκBα following treatment with Pg LPS and OMVs

Inhibitory effects of hBD3 and CA-074Me on the NF-κB activation induced by *Pg* LPS and OMVs were further evaluated by immunoblot analyses of IκBα degradation. The mean level of IκBα was significantly decreased in BV-2 microglia at 10-30 min after treatment with either *Pg* LPS (10 μg/mL) or OMVs (150 μg/mL). Both hBD3 (1 μM) and CA-074Me (30 μM) significantly inhibited IκBα degradation induced by *Pg* LPS in BV-2 microglia (Figures 6A,B). In contrast, neither hBD3 (1 μM) nor CA-074Me (30 μM) affected the IκBα degradation induced by OMVs (Figures 6C,D).

Preprints (www.preprints.org) | NOT PEER-REVIEWED | Posted: 26 December 2023 doi:10.20944/preprints202312.1924.v1

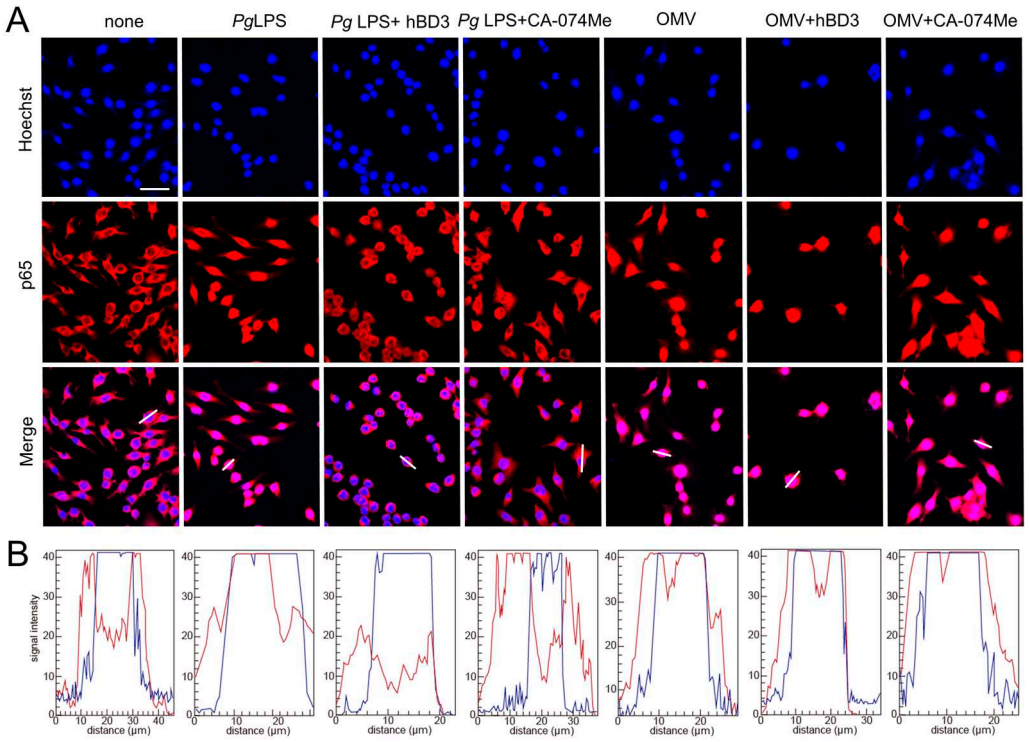

Figure 5. Effects of hBD3 and CA-074Me on nuclear NF-κB p65 translocation following stimulation with *Pg* LPS and OMVs. (**A**) Immunofluorescent CLSM images of BV-2 microglia after treatment with *Pg* LPS or OMVs in the absence or presence of hBD3 (1 μM) or CA-074Me (10 μM). Nuclear NF-κB p65 translocation was visualized by immunohistochemical staining (red). Nuclei were stained blue by Hoechst 33342 (blue). Scale bar = 40 μm. (**B**) The typical cells were analyzed by line plot profile to show the cytosol and nuclear NF-κB p65 translocation. indicate The fluorescence intensity of NF-κB p65 and Hoechst 33342 in the cells traversed by white lines in (**A**) was indicated by red and blue lines, respectively.

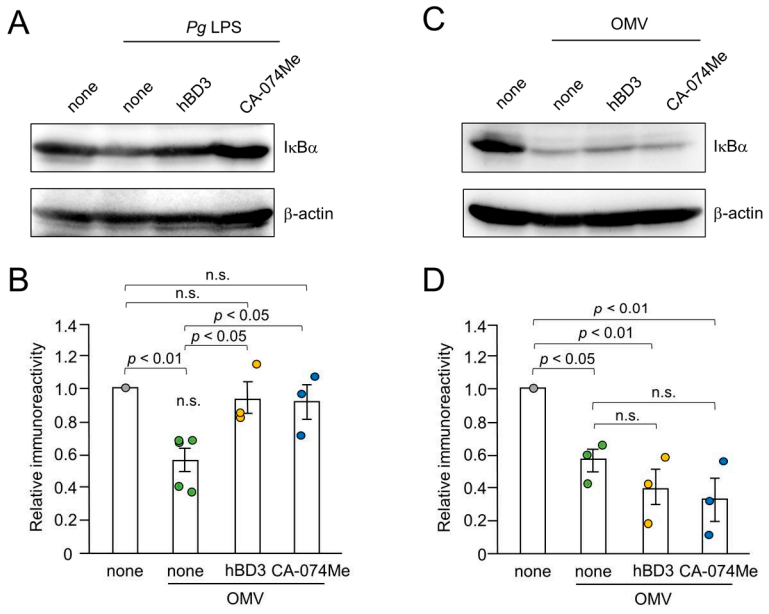

Figure 6. Effects of hBD3 and CA-074Me on the degradation of IκB*α* following treatment with *Pg* LPS and OMVs. (**A**) The protein expression of IκB*α* in BV-2 microglia after stimulation with *Pg* LPS (10 μg/mL) for 30 min in the presence or absence of hBD3 (1 μM) or CA-074Me (30 μM). (**B**) The mean

Preprints (www.preprints.org) | NOT PEER-REVIEWED | Posted: 26 December 2023 doi:10.20944/preprints202312.1924.v1

values of the IκBα intensity, which were detected by the immunoblots shown in (**A**), were measured and normalized against the signal of β-actin. The data relative to the values in un treated cells are presented as the mean ± SE of three-five independent experiments. The *p* values were calculated using a one-way ANOVA with a post-hoc Tukey's test. A value of $p<0.05$ was considered to indicate statistical significance. (**C**) The protein expression of IκBα in BV-2 microglia after stimulation with OMVs (150 μg/mL) for 10 min in the presence or absence of hBD3 (1 μM) or CA-074Me (30 μM). (**D**) The mean values of the IκBα intensity, which were detected by the immunoblots shown in (**C**), were measured and normalized against the signal of β-actin. The data relative to the values in untreated cells are presented as the mean ± SE of three independent experiments. The *p* values were calculated using a one-way ANOVA with a post-hoc Tukey's test. A value of $p<0.05$ was considered to indicate statistical significance.

3.7. Prediction of hBD3 binding to CatB and CatL

To examine the possibility that hBD3 inhibits the activities of CatB and CatL through direct binding, a high-quality model of hBD3-bound CatB was generated using AlphaFold (Figures 7A,B). The CatB model in the complex had a median predicted Local Distance Difference Test (pLDDT) score of 95.54 for 257 Cα atoms, except for 3 residues at *C*-terminus (Glu258-Ile260) (Figure 7A). The hBD3 model in the complex had a median pLDDT score of 87.48 for 45 Cα atoms, which included 2 residues with low confidence in the loop between the β1 and β2 strands, Arg36 (68.00) and Gly37 (66.69) (Figure 7A). In addition, the predicted alignment error (PAE) between CatB and hBD3 was extremely low (Figure 7B). Therefore, the complex model is reliable for analyzing the interactions between proteins. In the CatB model, an active-site cleft is formed on the molecular surface. At the bottom, the substrate-binding pocket, consisting of S1-S3, S1′ and S2′ sites, are lined across the catalytic Cys29 residue (Figure 7C).

In the complex model, the first half (Cys18-Cys23) of the loop between the α1 helix and β1 strand of hBD3 was inserted into the cleft of CatB toward the S2 site, while the other half (Cys23-Lys26) is inserted toward the S3 site (Figure 7C). Therefore, the CatB:hBD3 complex model suggests that hBD3 may inhibit enzymatic activity by blocking the substrate-binding pocket in the cleft of CatB.

On the other hand, the interaction between hBD3 and CatL, the model of hBD3-bound CatL indicates that hBD3 binds to the active cleft formed on the molecular surface of CatL (Figure 8A,B). However, the confidence level was relatively low (Figure 8C).

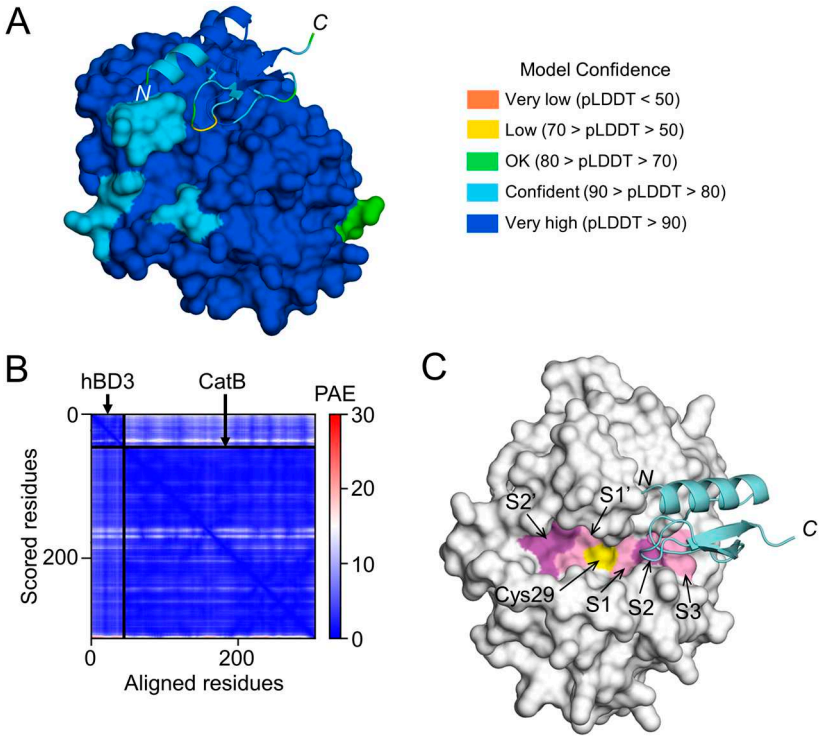

Preprints (www.preprints.org) | NOT PEER-REVIEWED | Posted: 26 December 2023 doi:10.20944/preprints202312.1924.v1

Figure 7. Prediction of hBD3 binding to CatB. (**A**) Structural model of hBD3-bound CatB generated using AlphaFold. The hBD3 model, presented as a ribbon, binds to the molecular surface of CatB. Amino acids are colored based on their pLDDT score. (**B**) PAE plots of the hBD3 and CatB complex model. (**C**) Binding of hBD3 to the active cleft formed on the molecular surface of CatB. The surface representation of CatB is shown in gray, except for the S1, S3, and S1′ sites, which are shown in light magenta; the S2 and S2′ sites, which are shown in magenta; and Cys29, which is shown in yellow. The hBD3 model, presented as a ribbon, is colored cyan. The figures were drawn using the PyMOL software program [50].

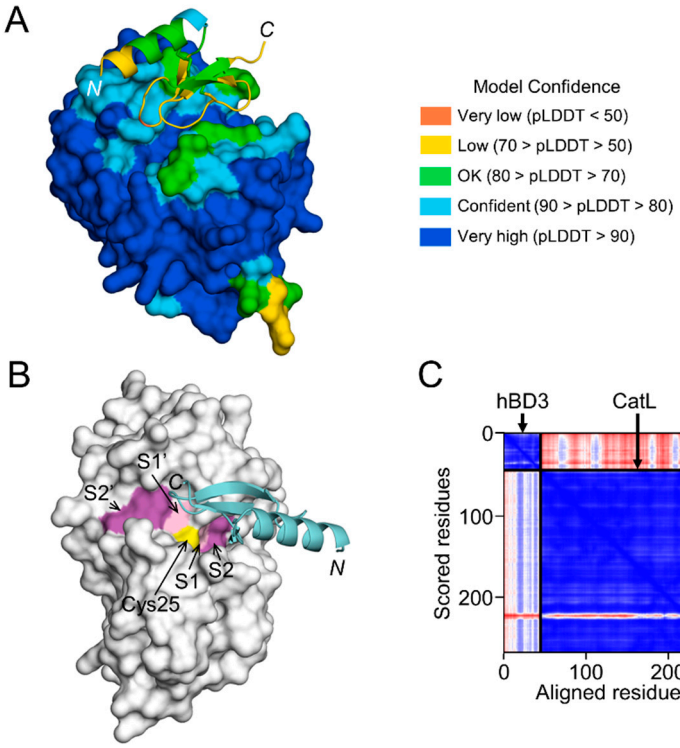

Figure 8. Prediction of hBD3 binding to CatL. (**A**) Structural model of hBD3-bound CatL generated using AlphaFold. hBD3 model, presented as a ribbon, binds to the molecular surface of CatL. Amino acids are colored based on their pLDDT score. (**B**) Binding of hBD3 to the active cleft formed on the molecular surface of CatL. The surface representation of CatL is shown in gray, except for S1 and S1′sites, which are shown in light magenta; the S2 and S2′ sites, which are shown in magenta; and Cys25, which is shown in yellow. The hBD3 model, presented as a ribbon, is colored cyan. (**C**) PAE plots of the hBD3 and CatL complex model. The figures were drawn using the PyMOL software program [50].

4. Discussion

hBD3 significantly suppressed the IL-1β production induced by *Pg* LPS but not by OMVs, while CA-074Me significantly inhibited the IL-1β production induced by both *Pg* LPS and OMVs. Furthermore, both hBD3 and CA-074Me significantly inhibited *Pg* LPS-induced nuclear NF-κB p65 translocation and IκBα degradation. In contrast, neither hBD3 nor CA-074Me blocked OMV-induced nuclear NF-κB p65 translocation and IκBα degradation. CA-074 could have non-cathepsin off-target effects [9,34], which may be responsible for the inhibitory effect of CA-074Me on OMV-induced IL-1β production. On the other hand, ZRLR, a specific CatB inhibitor, had no effect on *Pg* virulence factor-induced IL-1β production. This was consistent with the results obtained using shRNA-mediated knockdown of CatB expression. These results suggest that *Pg* LPS induces the synthesis and processing of pro-IL-1β through CatB/CatL-dependent mechanisms, without activation of the NLRP3 inflammasome. In contrast, OMVs may promote the synthesis and processing of pro-IL-1β through CatB/CatL-independent phagocytic mechanisms.

 doi:10.20944/preprints202312.1924.v1

The structural models generated by AlphaFold in this study indicated that hBD3 can bind more strongly to the substrate-binding pocket of CatB than to that of CatL, suggesting that hBD3 can more potently inhibit the enzymatic activity of CatB than that of CatL. This is consistent with our previous observations that hBD3 (1 μM) inhibits the enzymatic activities of human recombinant CatB and CatL by approximately 60% and 10%, respectively [21]. It was reported that hBD3 can be a substrate for cysteine cathepsins such as CatB and CatL [35]. Therefore, the present findings extend our previous implication that hBD3 suppresses *Pg* LPS-induced oxidative and inflammatory responses in microglia through the suicide substrate-based inhibition of CatB and CatL.

The methyl ester of CA-074Me is considered to be hydrolyzed by intracellular esterases releasing the active inhibitor, CA-074. However, the amount of CA-074 released into BV-2 microglia after treatment with CA-074Me remains unclear. Activity-based cysteine protease labeling using DCG-04 showed that CA-074Me is not a CatB-specific inhibitor in murine fibroblasts [36]. Therefore, CA-074Me may inhibit CatB and other cysteine cathepsins, especially CatL, at the concentrations used in previous studies (e.g. 10-30 μM). In contrast, ZRLR is a highly potent, irreversible, membrane-permeable, CatB-specific inhibitor. ZRLR is an azapeptide, which are peptide analogs in which the α-CH group of one amino acid resides in the peptide and is replaced by a nitrogen atom. The intrinsic structural prevalence of the *N*-terminal part of ZRLR is to remain bent, which allows a covalent attachment of ZRLR onto the active site Cys29 in CatB [37]. ZRLR exclusively blocks CatB in living primary antigen-presenting cells, in contrast to CA-074Me, by use of DCG-4, which detects active cysteine cathepsins in an activity- based reaction [33].

Currently, OMVs are considered to be potent vehicles for transmitting virulence factors into the host cells [38]. OMVs contain gingipains, which covalently bind to anionic LPS on their surface [32]. Furthermore, gingipains can activate pro-caspase-1 [39]. However, it is unlikely that the enzymatic activities of gingipains are involved in the IL-1β production, as pharmacological inhibition of both Kgp and Rgp did not block OMV-induced IL-1β production by BV-2 microglia. Our observations here showed that BV-2 microglia did not phagocytose OMVs prepared from KDP136, which is devoid of both Kgp and Rgp. It was reported that Rgp is necessary for the fimbriae formation [40,41]. Therefore, BV-2 microglia could not phagocytose OMVs prepared from KDP136 because of a lack of fimbriae, which is necessary for a lipid raft-mediated endocytic pathway [30,42]. Of particular note, OMVs prepared from KDP136 did not induce the IL-1β production by BV-2 microglia.

OMVs secreted by Gram-negative bacteria function as a vehicle that delivers LPS into the cytosol and induces caspase-11-dependent inflammatory responses [43,44]. It has been suggested that a functional interaction between caspase-11 and the NLRP3 inflammasome, and perhaps involving additional partners, could promote noncanonical activation of the pro-IL-β processing [45]. It has been reported that phagocytic machinery can activate NF-κB in macrophages [46] and monocytes [47]. We previously reported that OMVs can deliver gingipains into the cytosol of hCMEC/D3 cells [48]. However, whether or not *Pg* LPS released into the cytosol is involved in the IL-1β production by BV-2 microglia after phagocytosis of OMVs remains unclear. The precise CatB/CatL -independent mechanisms involved in OMV-induced IL-1β production by BV-2 microglia should be elucidated in future studies.

5. Conclusions

The abnormal expression and/or regulation of salivary antimicrobial peptides has been suggested to be associated with AD [49]. The present results suggest that hBD3, a salivary antimicrobial peptide, can improve the IL-1β-associated vicious inflammatory cycle induced by *Pg* LPS-stimulated microglia. Therefore, hBD3 may be a potential pharmacological intervention for the treatment of patients with sporadic AD, especially those with severe periodontitis.

Author Contributions: Conceptualization, H.N.; investigation, E.I., S.M., S.S, S.M., M.J., K.O., and S.N.; analysis, E.I., S.M., K.O., S.N., and H.N.; writing—original draft preparation, K.O., S.N., and H.N.; writing—review and editing, H.N.; and funding acquisition, H.N. All authors have read and agreed to the published version of the manuscript.

Funding: This work was supported by the Science Research Promotion Fund from the Promotion and Mutual Aid Cooperation for Private Schools of Japan (H.N.), and JSPS KAKENHI Grant Numbers JP21K06383 (H.N.).

Institutional Review Board Statement: The study was conducted in accordance with the guidelines of the Declaration of Helsinki, and approved by the Review Board for Animal Experiments of Yasuda Women's University.

Conflicts of Interest: The authors have no financial conflicts of interest to declare.

Data Availability Statement: The data that suport the findings of this study are available from the corresponding author (H.N.), upon reasonable request.

References

1. McGeer PL, McGeer EG. The amyloid cascade-inflammatory hypothesis of Alzheimer's disease: implications for therapy. *Acta Neuropathol*. **2013**, 126, 479-497. https://doi.org/10.1007/s0041-013-1177-7.
2. McGeer PL, Rogers J, McGeer EG. Inflammation, anti-inflammatory agents, and Alzheimer's disease: The last 22 years. *J Alzheimers Dis*. **2016**, 54, 853-857. https://doi.org/10.3233/JAD-160488.
3. Sarlus H, Heneka MT. Microglia in Alzheimer's disease. *J Clin Invest*. **2017**, 127, 3240-3249. https://doi.org/10.1172/JCI90606.
4. Kaneko N, Kurata M, Yamamoto T, Morikawa S, Masumoto J. The role of interleukin-1 in general pathology. *Inflamm Regen*. **2019**, 39, 12. https://doi.org/10.1186/s41232-019-0101-5.
5. Lopez-Castejon G, Brough D. Understanding the mechanism of IL-1β secretion. *Cytokine Growth Factor Rev*. **2011**, 22, 189-195. https://doi.org/10.1016/j.cytogfr.2011.10.001.
6. Ghosh S, Wu MD, Shaftel SS, Kyrkanides S, LaFerla FM, Olschowka JA, O'Banion MK. Sustained interleukin-1β overexpression exacerbates tau pathology despite reduced amyloid burden in an Alzheimer's mouse model. *J Neurosci.* **2013**, 33, 5053-5064. https://doi.org/10.1523/JNEUROSCI.4361-12.2013.
7. Bai H, Yang B, Yu W, Xiao Y, Yu D, Zhang Q. Cathepsin B links oxidative stress to the activation of NLRP3 inflammasome. *Exp Cell Res.* **2018**, 362, 180-187. https://doi.org/10.1016/j.yexcr.2017.11.015.
8. Chevriaux A, Pilot T, Derangère V, Simonin H, Martine P, Chalmin F, Ghiringhelli F, Rèbè C. Cathepsin B is required for NLRP3 inflammasome activation in macrophages, through NLRP3 interaction. *Front Cell Dev Biol.* **2020**, 8, 167. https://doi.org/10.3389/fcell.2020.00167.
9. Orlowski GM, Colbert JD, Sharma S, Bogyo M, Robertson SA, Rock KL. Multiple cathepsins promote pro-IL-β synthesis and NLRP3-mediated IL-1β activation. *J Immunol*. **2015**, 195, 1685-1697. https://doi.org/10.4049/jimmunol.1500509.
10. Campden RI, Zhang Y. The role of lysosomal cysteine cathepsins in NLRP3 inflammasome activation. *Arch Biochem Biophys.* **2019**, 670, 32-42. https://doi.org/10.1016/j.abb.2019.02.015.
11. Terada K, Yamada J, Hayashi Y, Wu Z, Uchiyama Y, Peters C, Nakanishi H. Involvement of cathepsin B in processing and secretion of interleukin-1β in chromogranin A-stimulated microglia. *Glia*, **2010**, 58, 114-124. https://doi.org/10.1002/glia.20906.
12. Sun L, Wu Z, Hayashi Y, Peters C, Tsuda M, Inoue K, Nakanishi H. Microglial cathepsin B contributes to the initiation of peripheral inflammation-induced chronic pain. *J. Neurosci*. **2012**, 32, 11330–11342. doi:10.1523/JNEUROSCI.0677-12.2012.
13. Colleran A, Ryan A, O'Gorman A, Mureau C, Liptrot C, Dockery P, Fearnhead H, Egan LJ. Autophagosomal IκBα degradation plays a role in the long term control of tumor necrosis factor-α-induced nuclear factor-κB (NF-κB) activity. *J Biol Chem.* **2011**, 286, 22886-22893. https://doi.org/10.1074/jbc.M110.199950.
14. Criollo A, Chereau F, Malik SA, Niso-Santano M, Mariño G, Galluzzi L, Maiuri MC, Baud V, Kroemer G. Autophagy is required for the activation of NF-κB. *Cell Cycle*. **2012**, 11, 194-199. https://doi.org/10.4161/cc.11.1.18669.
15. Ni J, Wu Z, Peterts C, Yamamoto K, Qing H, Nakanishi H. The critical role of proteolytic relay through cathepsins B and E in the phenotypic change of microglia/macrophage. *J Neurosci.* **2015**, 9, 35, 12488–12501. https://doi.org/10.1523/JNEUROSCI.1599-15.2015
16. Nakanishi H. Cathepsin regulation on microglial function. *Biochim Biophys Acta Proteins Proteom.* **2020**, 1868, 140465. https://doi.org/10.1016/j.bbapap.2020.140465.
17. Nakanishi H. Microglial cathepsin B as a key driver of inflammatory brain disease and brain aging. *Neural Regen Res.* **2020**, 15, 25-29. https://doi.org/10.4103/1673-5374.264444.
18. Kamer AR, Dasanayake AP, Craig RG, Glodzik-Sobanska L, Bry M, de Leon MJ. Alzheimer's disease and peripheral infections: the possible contribution from periodontal infections, model and hypothesis. *J Alzheimers Dis*. **2008**, 13:437-449. https://doi.org/10.3233/jad-2008-13408.
19. Welling MM, Nabuurs RJ, van der Weerd L. Potential role of antimicrobial peptides in the early onset of Alzheimer's disease. *Alzheimers Dement*. **2015**, 11, 51-57. https://doi.org/10.1016/j.jalz.2013.12.020.

20. De Smet K, Contreras R. Human antimicrobial peptides: defensins, cathelicidins and histatins. *Biotechnol Lett.* **2005**, 18, 1337-1347. https://doi.org/10.1007/s10529-005-0936-5.
21. Inoue E, Minatozaki S, Katsuta Y, Nonaka S, Nakanishi H. Human β-defensin 3 inhibits *Porphorymonas gingivalis* lipopolysaccharide-induced oxidative and inflammatory response of microglia by suppression of cathepsins B and L. *Int J Mol Sci*. **2022**, 23:15099. https://doi.org/10.3390/ijms232315099.
22. Wu Z, Ni J, Liu Y, Teeling JL, Takayama F, Collcutt A, Ibbett P, Nakanishi H. Cathepsin B plays a critical role in inducing Alzheimer's disease-like phenotypes following chronic systemic exposure to lipopolysaccharide from *Porphyromonas gingivalis* in mice. *Brain Behav. Immun.* **2017**, 65, 350–361. https://doi.org/10.1016/j.bbi.2017.06.002.
23. Gong T, Chen Q, Mao H, Zhang Y, Ren H, Xu M, Chen H, Yang D. Outer membrane vesicles of *Porphyromonas gingivalis* trigger NLRP3 inflammasome and induce neuroinflammation, tau phosphorylation, and memory dysfunction in mice. *Front Cell Infect Microbiol*. **2022**, 12, 925435. https://doi.org/10.3389/fcimb.2022.925435.
24. Blasi E, Barluzzi R, Bocchini V, Mazzolla R, Bistoni F. Immortalization of murine microglial cells by a v-raf/v-myc carrying retrovirus. *J Neuroimmunol.* **1990**, 27, 229-237. https://doi.org/10.1016/0165-5728(90)90073-v.
25. Henn A, Lund S, Hedtjärn M, Schrattenholz A, Pörzgen P, Leist M.The suitability of BV2 cells as alternative model system for primary microglia cultures or for animal experiments examining brain inflammation. *ALTEX*. **2009**, 26, 83-94. https://doi.org/10.14573/altex.2009.2.83.
26. Timmerman R, Burm SM, Bajramovic JJ. An overview of *in vitro* methods to study microglia. *Front Cell Neurosci*. **2018**, 12:242. https://doi.org/10.3389/fncel.2018.00242.
27. Tozaki-Saitoh H, Sasaki I, Yamashita T, Hosoi M, Kato TA, Tsuda M. Involvement of exchange protein directly activated by cAMP and tumor progression locus 2 in IL-1β production in microglial cells following activation of β-adrenergic receptors. *J Pharmacol Sci*. 2020, 142, 133-140. https://doi.org/10.1016/j.jphs.2020.03.004.
28. Afonina IS, Muller C, Martin SJ, Beyaert R. Proteolytic processing of interleukin-1 family cytokines: variations on a common theme. *Immunity* **2015**, 42, 991-1004. https://doi.org/10.1016/j.immuni.2015.06.003.
29. Seyama M, Yoshida K, Yoshida K, Fujiwara N, Ono K, Eguchi T, Kawai H, Guo J, Weng Y, Haoze Y, Uchibe K, Ikegame M, Sasaki A, Nagatsuka H, Okamoto K, Okamura H, Ozaki K. Outer membrane vesicles of *Porphyromonas gingivalis* attenuate insulin sensitivity by delivering gingipains to the liver. *Biochim Biophys Acta Mol Basis Dis*. **2020**, 1866, 165731. https://doi.org/10.1016/j.bbadis.2020.165731.
30. Furuta N, Takeuchi H, Amano A. Entry of *Porphyromonas gingivalis* outer membrane vesicles into epithelial cells causes cellular functional impairment. *Infect Immun*. **2009**, 77, 4761-4770. https://doi.org/10.1128/IAI.00841-09.
31. Mirdita M, Schütze K, Moriwaki Y, Heo L, Ovchinnikov S, Steinegger M. ColabFold: Making protein folding accessible to all. *Nature Methods*. **2022**, 19, 679-682. https://doi.org/10.1038/s41592-022-01488-1.
32. Shoji M, Sato K, Yukitake H, Kondo Y, Narita Y, Kadowaki T, Naito M, Nakayama K. Por secretion system-dependent secretion and glycosylation of *Porphyromonas gingivalis* hemin-binding protein 35. *PLoS One*. **2011**, 6, e21372. https://doi.org/10.1371/journal.pone.0021372.
33. Reich M, Wieczerzak E, Jankowska E, Palesch D, Boehm BO, Burster T. Specific cathepsin B inhibitor is cell-permeable and activates presentation of TTC in primary human dendritic cells. *Immun Lett*. **2009**, 123, 155-159. https://doi.org/10.1016/j.imlet.2009.03.006.
34. Patel N, Nizami S, Song L, Mikami M, Hsu A, Hickernell T, Chandhanayingyong C, Rho S, Compton JT, Caldwell JM, Kaiser PB, Bai H, Lee HG, Fischer CR, Lee FY. CA-074Me compound inhibits osteoclastogenesis via suppression of the NFATc1 and c-FOS signaling pathways. *J Orthop Res*. **2015**, 33, 1474-1486. https://doi.org/10.1002/jor.22795.
35. Taggart CC, Greene CM, Smith SG, Levine RL, McCray PB, Jr, O'Neill S, McElvaney NG. Inactivation of human β-defensins 2 and 3 by elastolytic cathepsins. *J. Immunol.* **2003**, 171, 931-937. https://doi.org/10.4049/jimmunol.171.2.931.
36. Montaser M, Lalmanach G, Mach L. CA-074, but not its methyl ester CA-074Me, is a selective inhibitor of cathepsin B within living cells. *Biol Chem*. **2002**, 383, 1305–1308. https://doi.org/10.1515/BC.2002.147.
37. Wieczerzak E, Rodziewicz-Motowidlo S, Jankowska E, Gieldoń A, Ciarkowski J. An enormously active and selective azapeptide inhibitor of cathepsin B. *J Pept Sci*. **2007**, 13, 536–643. https://doi.org/10.1002/psc.883.
38. Okamura H, Hirota K, Yoshida K, Weng Y, He Y, Shiotsu N, Ikegame M, Uchida-Fukuhara Y, Tanai A, Guo J. Outer membrane vesicles of *Porphyromonas gingivalis*: Novel communication tool and strategy. *Jpn Dent Sci Rev*. **2021**, 57, 138-146. https://doi.org/10.1016/j.jdsr.2021.07.003.
39. Jung YJ, Jun HK, Choi BK. Contradictory roles of *Porphyromonas gingivalis* gingipains in caspase-1 activation. *Cell Microbiol*. **2015**, 17, 1304-1319. https://doi.org/10.1111/cmi.12435.
40. Kadowaki T, Nakayama K, Yoshimura F, Okamoto K, Abe N, Yamamoto K. Arg-gingipain acts as a major processing enzyme for various cell surface proteins in *Porphyromonas gingivalis*. *J Biol Chem*. **1998**, 273, 29072-29076. https://doi.org/10.1074/jbc.273.44.29072.

41. Shibata S, Shoji M, Okada K, Matsunami H, Matthews MM, Imada K, Nakayama K, Wolf M. Structure of polymerized type V pilin reveals assembly mechanism involving protease-mediated strand exchange. *Nat Microbiol*. **2020**, 5, 830-837. https://doi.org/10.1038/s41564-020-0705-1.
42. Zhang Z, Liu D, Liu S, Zhang S, Pan Y. The role of *Porphyromonas gingivalis* outer membrane vesicles in periodontal disease and related systemic diseases. *Front Cell Infec Microbiol*. **2021**, 10, 585917. https://doi.org/10.3389/fcimb.2020.585917.
43. Vanaja SK, Russo AJ, Behl B, Banerjee I, Yankova M, Deshmukh SD, Rathinam VAK. Bacterial outer membrane vesicles mediate cytosolic localization of LPS and caspase-11 activation. *Cell*, **2016**, 165, 1106-1119. doi:10.1016/j.cell.2016.04.015.
44. Finethy R, Dockterman J, Kutsch M, Orench-Rivera N, Wallace GD, Piro AS, Luoma S, Haldar AK, Hwang S, Martinez J, Kuehn MJ, Taylor GA, Coers J. Dynamin-related Irgm proteins modulate LPS-induced caspase-11 activation and septic shock. *EMBO Rep*. **2020**, 21:e50830. https://doi.org/10.15252/embr.202050830.
45. Moretti J, Blander JM. Increasing complexity of NLRP3 inflammasome regulation. *J Leuko Biol*, **2021**, 109, 561-571. https://doi.org/10.1002/JLB.3MR0520-104RR.
46. Muroi M, Muroi Y, Suzuki T. The binding of immobilized IgG2a to Fcγ2a receptor activates NF-κB via reactive oxygen intermediates and tumor necrosis factor-α1. *J Biol Chem*. **1994**, 269, 30561-30568.
47. Thieblemont N, Haeffner-Cavaillon N, Haeffner A, Cholley B, Weiss L, Kazatchkine MD. Triggering of complement receptors CR1(CD35) and CR3 (CD11b/CD18) induces nuclear translocation of NF-κB (p50/p65) in human monocytes and enhances viral replication in HIV-infected monocytic cells. *J Immuniol*. **1995**, 155, 4861-4867.
48. Nonaka S, Kadawaki T, Nakanishi H. Secreted gingipains from *Porphyromonas gingivalis* increase permeability in human cerebral microvascular endothelial cells through intracellular degradation of tight junction proteins. *Neurochem Int*. **2022**, 154, 105282. https://doi.org/10.1016/j.neuint.2022.105282.
49. Contini C, Olianas A, Serrao S, Deriu C, Iavarone F, Boroumand M, Bizzarro A, Lauria A, Faa G, Castagnola M, Messana I, Manconi B, Masullo C, Cabras T. Top-down proteomics of human saliva highlights anti-inflammatory, antioxidant, and antimicrobial defense responses in Alzheimer disease. *Front. Neurosci.* **2021**, 15, 668852. https://doi.org/10.3389/fnins.2021.668852.
50. DeLano WL. The PyMOL molecular graphics system. *DeLano Scientific*, San Carlos, CA., **2002**.